articles

Solution structure of Ca²⁺–calmodulin reveals flexible hand-like properties of its domains

James J. Chou[1], Shipeng Li[2], Claude B. Klee[2] and Ad Bax[1]

The solution structure of Ca²⁺-ligated calmodulin is determined from residual dipolar couplings measured in a liquid crystalline medium and from a large number of heteronuclear J couplings for defining side chains. Although the C-terminal domain solution structure is similar to the X-ray crystal structure, the EF hands of the N-terminal domain are considerably less open. The substantial differences in interhelical angles correspond to negligible changes in short interproton distances and, therefore, cannot be identified by comparison of NOEs and X-ray data. NOE analysis, however, excludes a two-state equilibrium in which the closed apo conformation is partially populated in the Ca²⁺-ligated state. The difference between the crystal and solution structures of Ca²⁺–calmodulin indicates considerable backbone plasticity within the domains of calmodulin, which is key to their ability to bind a wide range of targets. In contrast, the vast majority of side chains making up the target binding surface are locked into the same χ_1 rotameric states as in complexes with target peptide.

Calmodulin (CaM) is a ubiquitous Ca²⁺ binding protein that plays a key role in numerous cellular Ca²⁺-dependent signaling pathways[1]. It regulates the activity of a large array of different target autoinhibitory proteins, including protein kinases, ion channels and pumps, nitric-oxide synthases, adenylyl cyclases and phosphodiesterases. Ample evidence indicates that Ca²⁺–CaM activates these proteins through interactions with their activity-suppressing segments, which encompass peptide sequences with a high propensity for helix formation[2,3].

The crystal structure of Ca²⁺–CaM shows a pronounced dumbbell shape, with the N- and C-terminal domains separated by a 27-residue α-helical linker, often referred to as the 'central helix'[4]. The homologous (46% sequence identity) N- and C-terminal domains each consist of two EF hand-type Ca²⁺-binding helix-loop-helix motifs[5] that are paired by a mini-antiparallel β-sheet. In the presence of Ca²⁺, the interhelical angle in each EF hand is large, giving rise to a deep hydrophobic cleft between helices I–IV and II–III in each domain. The hydrophobic residues lining the insides of these clefts are key in determining the high affinity of CaM for a wide range of targets[6,7].

Although the 'central helix' linker of CaM in complex with Ca²⁺ is α-helical in the crystalline state, NMR relaxation data conclusively show that this linker is nonhelical and highly flexible near its mid-point[8]. The functional importance of this plasticity was highlighted by structures of CaM in complex with target peptides. In these complexes, the two CaM domains come together and clamp around the helical target peptide[9–11]. Clearly, the flexibility of the interdomain linker is key in allowing the two domains to come together and permitting rearrangement of the relative positions of the two domains to fit the wide array of target sites[11].

In the absence of Ca²⁺, the interdomain linker is considerably less flexible, resulting in an extended dumbbell structure and a highly anisotropic rotational diffusion of the protein in solution[12]. This makes it impossible for both domains to bind simultaneously to the same target peptide. Moreover, the
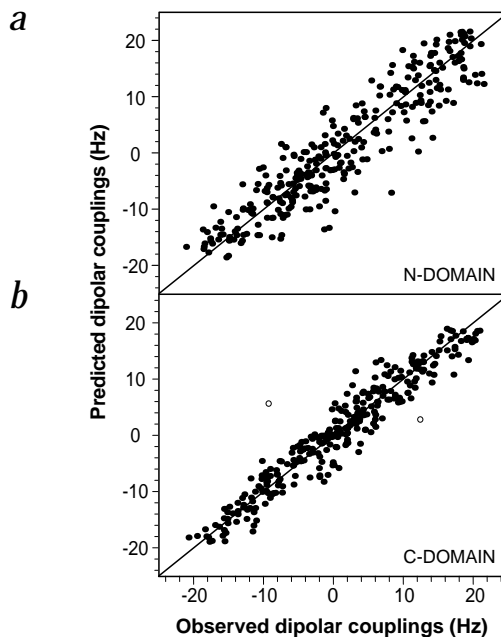
Fig. 1 Correlation between normalized observed backbone dipolar couplings (Table 1) and couplings predicted for the 1 Å X-ray structure of CaM (PDB entry 1EXR), using an alignment tensor obtained from the SVD fit. All dipolar couplings were measured in 15 mg ml⁻¹ Pf1 liquid crystal and 10 mM KCl, and are normalized to $^1D_{NH}$. **a**, For the N-terminal domain (residues 5–75), the correlation coefficient, R_{SVD}, equals 0.91, and Q is 41%. Alignment tensor relative to 1EXR: $D_a^{NH} = 10.8$ Hz and rhombicity, R, = 0.42. **b**, For the C-terminal domain (residues 82–146), $R_{SVD} = 0.97$ and Q = 25%, and $D_a^{NH} = -9.6$ Hz, R = 0.64. The two open circles represent $^1D_{NH}$ of Ile 130 and Asn 137, which were also included in the fit.

helices in each pair of EF hands are nearly antiparallel, resulting in a tight four-helical bundle[13–15], which is similar to that observed in the crystal structure of the N-terminal domain of troponin-C[16], the Ca²⁺-binding subunit of the troponin com-
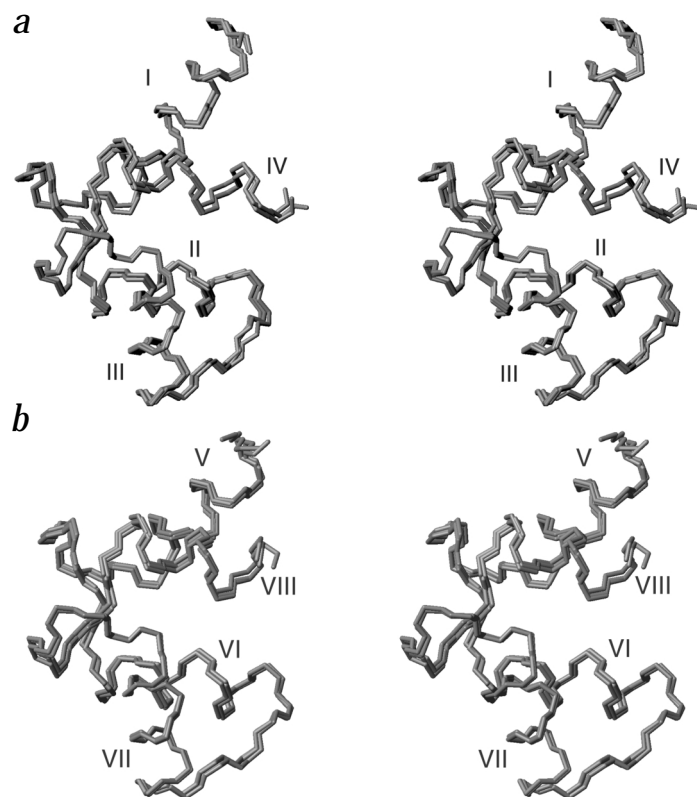
a

b

Fig. 2 Superposition of the lowest energy structures for *a*, the N-terminal domain (Thr 5–Arg 74) and *b*, the C-terminal domain (Glu 82 – Thr 146) of Ca²⁺–CaM, derived using three different starting structures: apo CaM (1F70 and 1F71), a parvalbumin-derived homology model and *Paramecium* Ca²⁺–CaM (1EXR). The backbone r.m.s. deviation relative to the mean is 0.24 Å.

tool to validate existing structural models[20–22]. In the current study, an extensive set of backbone dipolar couplings, including the one-bond ^1H-^{15}N, $^1H\alpha$-$^{13}C\alpha$, $^{13}C'_{i-1}$-N_i and $^{13}C\alpha$-$^{13}C'$, and the two-bond $^1H\alpha$-$^{13}C'$ couplings, were measured in a liquid crystalline medium consisting of 15 mg ml⁻¹ of the filamentous phage Pf1 (ref. 23). Such a Pf1 suspension provides a robust medium for alignment of negatively charged macromolecules. The best fits between these dipolar couplings and any of the PDB entries for CaM is obtained for *Paramecium tetraurelia* CaM (PDB entry 1EXR)[17] (Fig. 1). Although our NMR measurements were actually carried out on mammalian CaM, for which a 1.7 Å structure is available (PDB-entry 1CLL)[24], the lower uncertainty in the 1EXR atomic coordinates results in slightly better agreement with the dipolar couplings than is obtained for 1CLL. Nevertheless, even for the 1 Å structure, the correlation with the dipolar couplings is weaker than expected. The fits are performed separately for the N- and C-terminal domains of CaM because, owing to the high flexibility of the interdomain linker, the two domains align to different degrees. The fit for the N-terminal domain is particularly poor, corresponding to a correlation coefficient of the SVD fit (R_{SVD}) of 0.91, or a quality factor[20,22], Q, of 41%. For the C-terminal domain (residues 82–146), R_{SVD} equals 0.97 and Q = 25%, indicating better agreement between this domain in solution and in the crystalline lattice. The two main outliers in the C-terminal domain fit (open circles, Fig. 1*b*) correspond to $^1D_{NH}$ of Ile 130 and Asn 137. The Ile 130 N-H dipolar coupling also disagrees with all other CaM crystal structures in the database; however, this vector is unusually mobile in solution[8]. The Asn 137 N-H coupling is an outlier when compared with the 1EXR structure, but it agrees perfectly with the 1.7 Å crystal structure of mammalian CaM (PDB entry 1CLL)[24], possibly relating to the I136V sequence difference between *Paramecium* and mammalian CaM. Other minor outliers in the correlation for the C-terminal domain concern residues in the flexible loop region connecting helices VI and VII.
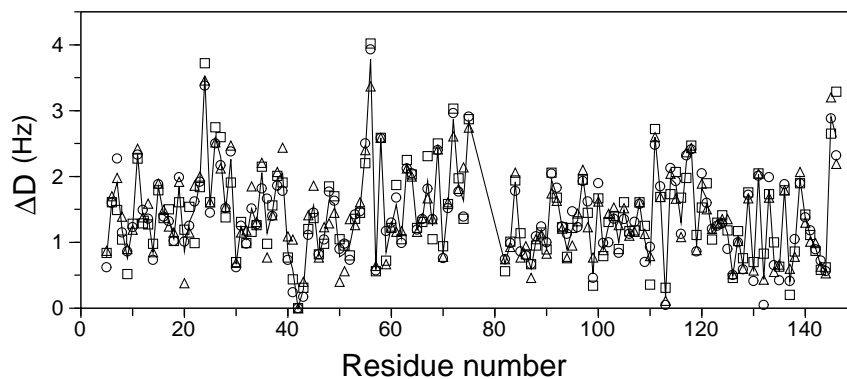
Structure determination from dipolar couplings

Calculating a structure from dipolar couplings presents a challenging multiple minimum problem, in part because the direction of an internuclear vector cannot be distinguished from its inverse. However, when a reasonable initial model is available, this degeneracy no longer constitutes a problem. We demonstrated that starting from the crystal structure of the Ca²⁺–CaM N-terminal domain, experimental ^1H-^{15}N, $^1H\alpha$-$^{13}C\alpha$ and $^{13}C'$-$^{13}C\alpha$ dipolar couplings measured for the apo form were sufficient to derive the apo CaM structure[25]. This structure calculation relied on a two-stage simulated annealing protocol carried out at low temperature. Here we use a slightly modified version of this protocol that additionally includes $^3J_{NC\gamma}$- and $^3J_{C'C\gamma}$-derived χ_1 and $^3J_{C\alpha C\delta}$-derived χ_2 rotamer restraints, and uses $^1H\beta$-$^{13}C\beta$ and $^{13}CH_3$ dipolar couplings to refine χ_1 and χ_2.

plex. In this conformation, the hydrophobic cleft has collapsed and is no longer accessible to target binding.

The 1 Å crystal structure of Ca²⁺–CaM shows that even at low temperature (100 K), the 'central helix' is subject to substantial anisotropic displacement relative to the rest of the protein. This structure also indicates plasticity within the individual domains[17]. No solution NMR structure for Ca²⁺-ligated intact CaM has been published, although observed NOE patterns were reported to be consistent with the crystal structure[18], implying a very similar structure. The solution structure of an engineered C-terminal domain of CaM was found to be approximately similar to the crystal structure, indicating that each domain constitutes an autonomous structural unit[15]. However, conventional NMR structure determination is based on the measurement of semiquantitative distances between pairs of protons that are separated by <4 Å. Without measurable interproton distances between the ends of the helices in the V-shaped open EF hand, accurate determination of the relative helix orientations is problematic.

We show that orientational information contained in residual dipolar couplings, which are easily measured by dissolving the protein in a dilute liquid crystalline phase[19], can readily solve this problem. Five dipolar couplings per residue define the structure of the protein very tightly and also allow extensive crossvalidation. For the N-terminal domain of Ca²⁺–CaM, we find remarkably large differences relative to all eukaryotic CaM X-ray structures, all derived from P1 space group crystals. Macromolecular structure determination from dipolar couplings is a very direct and rapid process. Some strengths and weaknesses of this novel approach will be emphasized.

Correlation of dipolar couplings and crystal structure

Other than their use as input parameters in NMR structure calculation, dipolar couplings provide a very direct and simple

articles

Fig. 3 Normalized average difference, ΔD, between the measured dipolar couplings and those predicted by the refined NMR structure as a function of residue number. $\Delta D = (((\Delta^1 D_{NH})^2 + (\Delta^1 D_{C\alpha H\alpha})^2 + (\Delta^1 D_{C'C\alpha})^2 + (\Delta^1 D_{C'N})^2 + (\Delta^2 D_{C'H\alpha})^2) / 5)^{1/2}$ represents the normalized r.m.s. difference between measure and best-fit couplings, where all couplings have been normalized relative to $^1 D_{NH}$. No couplings were measured for Asn 42 because residue 43 is a Pro and Asn 42 HN is broadened by rapid solvent exchange at pH 7.0. Residues Met 76–Asp 81 are highly flexible and excluded from the structure calculation. The symbols correspond to apo CaM (square), parvalbumin (triangle) and Ca²⁺–CaM (circle) starting structures.

Three different starting models are used: (i) the 1 Å crystal structure (1EXR); (ii) the solution structure of apo CaM (1F70 and 1F71)[25], which differ from 1EXR by ~4.5 Å for each of the two domains; and (iii) homology models built, using the program GeneMine[26], on the basis of the crystal structure of parvalbumin (51 and 70% similarity and 26 and 27% sequence identity for the N- and C-terminal domains, respectively). The structure calculation protocol consists of three stages. In the first stage, the backbone torsion angles are harmonically restrained to remain close to those of the starting model, but a gradual increase in the dipolar energy term forces larger ordered elements, such as α-helices, into the right orientation. In the second stage, this procedure is essentially repeated, but the backbone torsion angles are now harmonically restrained to the values of the lowest energy model obtained after the first stage. The force constant used in the backbone harmonic torsion restraint term is also ramped down during this second stage, allowing the structure to relax to a low energy conformation that satisfies the dipolar couplings. Side chains with well-defined torsion angles are harmonically restrained (with a ±30° tolerance) to their J coupling-derived values. In the third stage, the backbone is held largely constant by means of a noncrystallographic symmetry restraint term, and dipolar restraints for the side chains are introduced. All three starting models lead to very similar structures, demonstrating validity of the approach (Fig. 2; Table 1).

The vast majority of residues in the final structures satisfy the backbone dipolar restraints: with overall normalized root mean square (r.m.s.) deviations between structure and experimental data of 1.7 Hz for the N-terminal domain and 1.5 Hz for the C-terminal domain, agreement is good (Fig. 3). This final result is essentially independent of the starting structure, although for individual residues the final agreement with experimental data differs slightly when using the three different starting models. For a few residues (Gly 24, Val 55, Asp 56, Met 145 and Thr 146), below average agreement is observed consistently, independent of the starting model. These mostly correlate with higher than average internal backbone dynamics. Val 55 and Asp 56 backbone dynamics are not much above average; however, in the 1 Å resolution crystal structure, these residues show rather large deviations (8° and 9°) from peptide bond planarity. CaM crystal structures also differ in the χ_1 rotamer reported for Val 55, and the $^3 J_{NC\gamma}$ and $^3 J_{C'C\gamma}$ couplings indicate χ_1 rotamer averaging. This may be responsible for small backbone rearrangements, which are the likely source of our inability to define a single structure that fits the experimental data for these two residues.

Structure validation

An independent method to validate the structure is to compare dipolar couplings not used in the refinement with values pre-dicted by the structure[20–22]. For structures determined exclusively with dipolar couplings, this type of crossvalidation can sometimes be problematic because the total number of restraints is rather small relative to the number of degrees of freedom in the system[27]. However, in the present case, up to five backbone dipolar couplings are available for the majority of residues, which is sufficient to permit crossvalidation. For example, when calculating the structures without including two bond $^2 D_{C'H\alpha}$ restraints, these experimental values fit the experimental structure with correlation coefficients of $R_{SVD} = 0.98$, corresponding to Q_{free} factors of 18% and 20% for the N- and C-terminal domains, respectively. Similar Q-factors are obtained when omitting any of the other types of couplings. However, when simultaneously omitting two types of couplings (for example, $^2 D_{C'H\alpha}$ and $^1 D_{C\alpha H\alpha}$), the structural quality deteriorates ($R_{SVD} \approx 0.96$ and $Q \approx 30\%$). Even though the overall structures do not shift significantly (r.m.s. deviation of 0.44 Å) when simultaneously omitting two types of couplings, the local structure apparently becomes less accurate.

Could the liquid crystal affect CaM's structure?

The liquid crystals used in biological NMR are dilute aqueous suspensions of oriented particles, separated by many hundreds of Å. In the absence of an attractive potential between the protein and the particles, the vast majority of solute proteins are, therefore, far removed from the liquid crystal particles. However, the small fraction of time during which the protein diffuses to within a distance where the particle exerts a force on the protein (either electrostatically or sterically) contributes to the nonzero dipolar coupling. Therefore, the question of whether the liquid crystal could affect the structure is important.

The most compelling data against an effect of the liquid crystal on the protein are for T4 lysozyme. Goto *et al.*[28] showed that despite the flexibility of the linker, the relative domain orientation in T4 lysozyme is independent of the type of interaction (steric or electrostatic) with the liquid crystal, even though the average orientation of the protein relative to the two liquid crystals is quite different. For CaM, we have only a single alignment medium (Pf1) in which the sample remains stable indefinitely. CaM alignment in this medium is dominated by the strong repellant interaction between the negatively charged CaM and phage particles, essentially preventing direct contacts between them. The strength of the electrostatic repulsion can be altered by adjustment of the ionic strength. At high ionic strength (100 mM), the Debye-Hueckel electrostatic potential decreases steeply as a function of distance from the phage. In contrast, at low ionic strength this drop-off is much more shallow, and electrostatic repulsion causes the CaM con-
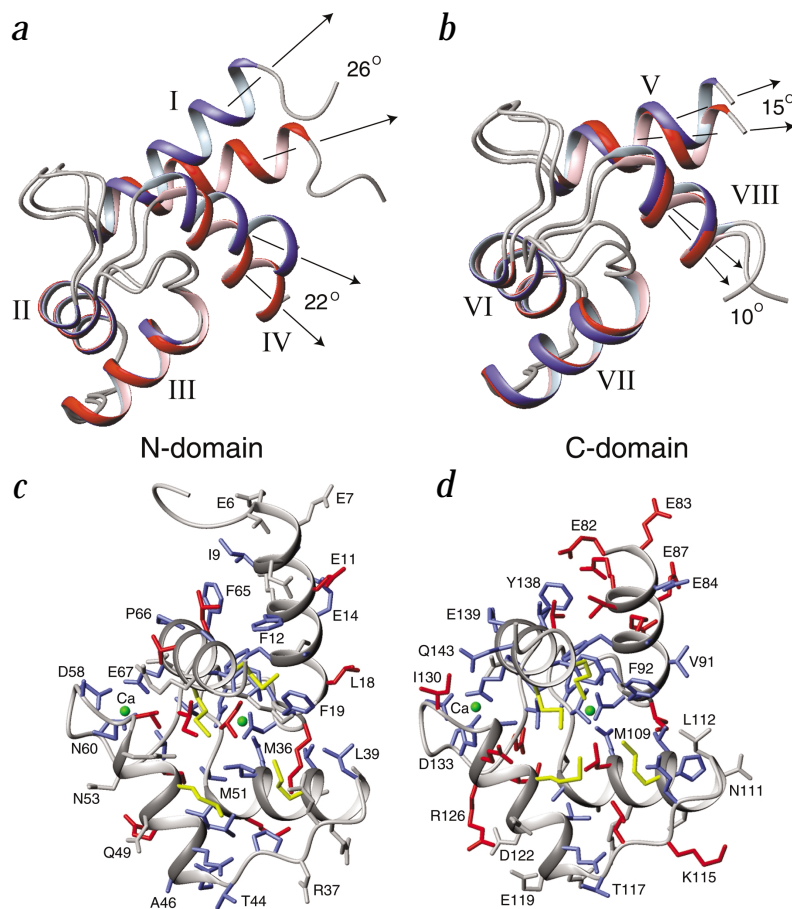
Fig. 4 Ribbon diagrams of the backbone of the Ca^{2+}–CaM solution structure, shown in red, and the 1 Å crystal structure (1EXR) in blue. ***a***, For the N-terminal domain, the superposition is optimized for residues 29–54 (helices II and III), revealing the large difference in the orientation of helix I (26°) and IV (22°). ***b***, For the C-terminal domain, residues 102–127 (helices VI and VII) are superimposed, showing much smaller orientation differences of 15° and 10° for helix V and VIII, respectively. ***c***,***d***, Solution structures including side chains, color coded according to their mobility as determined by $^3J_{CC}$ and $^3J_{CN}$ couplings. Red indicates extensive rotameric χ_1 averaging; blue, single χ_1 rotamers; and gray, residues with insufficient data for accurately defining χ_1 distributions. Eight Met residues (yellow) have unique χ_1 angles but exhibit extensive χ_3 averaging. Figures generated using MOLMOL[49].

centration within a 15 Å shell around the phage to be essentially zero. The data used in the present study were recorded at low ionic strength (10 mM). However, a nearly complete set of $^1D_{C'C\alpha}$ couplings was also collected at 100 mM KCl. At this higher ionic strength, we find, as expected, that the alignment tensor magnitude and orientation differ significantly from the values at 10 mM KCl; therefore, the $^1D_{C'C\alpha}$ couplings measured at 10 mM and 100 mM KCl correlate rather poorly with one another. Nevertheless, the 100 mM $^1D_{C'C\alpha}$ couplings fit the 10 mM Ca^{2+}–CaM structure as well ($R_{SVD} = 0.98$) as the dipolar couplings measured at 10 mM KCl, confirming that the structure of the protein is the same at the two ionic strengths. The strength and orientation of the electrostatic force on CaM are different at the two ionic strengths, but the CaM domain structures are the same, confirming the absence of an affect of the liquid crystal on the protein.

Structure comparison

The differences between the newly calculated NMR structures of the N- and C-terminal domains of Ca^{2+}–CaM and the 1 Å X-ray structure (1EXR) are best visible when the structures are overlaid such that the fit between helices II and III is optimized for the N-terminal domain, and similarly for helices VI and VII in the C-terminal domain (Fig. 4). For the C-terminal domain, the solution and crystal structures are quite similar, with an overall backbone r.m.s. deviation of 0.8 Å. Nevertheless, a 15° change in the orientation of helix V and a smaller change for helix VIII are clearly visible.

As expected from the poor SVD fit (Fig. 1*a*), the N-terminal domain in solution deviates significantly from that in the crys-

talline lattice (backbone r.m.s. deviation of 1.8 Å). Indeed, relative to the crystal structure, helices I and IV move closer towards the apo, or closed, form by 26° and 22°, respectively (Fig. 4*a*). The degree of hydrophobic cleft-opening is commonly characterized by the interhelical angles between the individual pairs of EF hand helices. Therefore, less 'open' is equivalent to smaller interhelical angles. Comparisons of the interhelical angles of the four EF hand motifs for the solution CaM structure and a number of different X-ray structures (Table 2) show that the two high-resolution X-ray structures of the free Ca^{2+}–CaM (1EXR and 1CLL) are very similar to each other — their EF-hand interhelical angles differ by <4°. However, for the N-terminal EF hands of both of these structures are significantly more 'open' than their corresponding C-terminal counterparts (Table 2). Remarkably, in the complex with a target peptide of CaM-dependent protein kinase IIα (PDB entry 1CDM)[11], the N-terminal domain becomes less open relative to 1EXR, whereas the opposite is seen for the C-terminal half. When associated with a target peptide of myosin light chain kinase (PDB entry 1CDL)[10], the reverse is seen.

When comparing the N- and C-terminal domains within each individual Ca^{2+}–CaM structure, structural similarity is higher in solution (backbone r.m.s. deviation 0.65 Å) than in the crystalline lattice (r.m.s. deviation 0.9 Å). Strong structural similarity is expected because the N- and C-terminal domains are 46% identical. Nevertheless, the alignment tensors for the two domains, and in particular the orientation of this tensor relative to each domain, differ considerably. This difference is caused primarily by the linker between the two domains, which for the N-terminal domain is at its C-terminal end; the inverse applies for the C-terminal domain. A simple steric picture, therefore, predicts large differences for a semiflexibly linked pair of identical domains[29].

The solution structure shows the smallest opening angles of any of the N-terminal domain Ca^{2+}–CaM structures, with interhelical angles that fall in between those of the crystal structure and the apo form, albeit considerably closer to those of the Ca^{2+}-ligated form. In terms of interhelical angles, the solution Ca^{2+}–CaM structure is closest to the angles seen in the 'semi-open' form, found for the C-terminal domains of the regulatory light chain (RLC) and essential light chain (ELC) when bound to IQ motifs of the regulatory domain of scallop myosin[30].

articles

Nearly all crystal structures of free Ca^{2+}–CaM were collected on crystals in the P1 space group. As noted by Wilson and Brunger[17], a fifth Ca^{2+} ion in this crystal forms an intermolecular salt bridge between Glu 47-Oϵ of one protein to Asp 58-Oδ of its neighbor, possibly contributing to the very large opening angle seen in the crystalline state. A CaM double deletion mutant, which crystallizes in the P21 space group, shows a considerably (10°) smaller I–II opening angle[31]. A second factor may be that the absence of a break between helices IV and V in the crystalline state, in contrast to the flexible linker observed between these helices in solution, affects the opening angles involving these helices.

Flexibility of side chains

Side chain mobility plays a key role in molecular recognition. Previous NMR studies of side chain dynamics in CaM have focused primarily on methyl group-containing residues[7]. In particular, much attention has focused on the importance of the inherent flexibility of the Met residues from CaM, eight of which are involved in target binding[7,32]. We have used heteronuclear $^3J_{NC\gamma}$ and $^3J_{C'C\gamma}$ couplings to determine which residues have side chains with well-defined χ_1 angles, and additional measurement of $^3J_{C\alpha C\delta}$ couplings in Ile and Leu residues for defining χ_2.

Measurement of $^3J_{NC\gamma}$ and $^3J_{C'C\gamma}$ couplings is relatively straightforward[33] and was carried out for all residues, except for a small fraction obscured by resonance overlap. All 10 aromatic residues, five of which are involved in contacting target peptide, are clearly locked into single rotameric states, identical to those found in the complex with target peptide[33]. Remarkably, all eight remaining Met residues, except for Met 76, also have unique χ_1 angles that are identical to those observed in the 1 Å crystal structure[17] and in the crystal structure with a target peptide[11]. In fact, in the free protein, we observe significant rotameric χ_1 averaging for only five out of 27 non-Ala, target-interacting residues (Glu 11, Leu 18, Ile 27, Val 55 and Leu 116). None of the remaining 22 residues shift from a well-defined rotameric state in the free protein to a different rotamer in the complex[11]. At first sight, this result contrasts with the NMR relaxation studies by Lee *et al.*[7], who noted a significant decrease in side chain entropy upon target binding. However, J(0) spectral density terms that define the order parameter in relaxation studies are much more sensitive to rotameric averaging than ^{13}C-^{13}C coupling constants, where the presence of averaging is difficult to establish if the dominant rotamer is occupied ≥80%. Also, analysis of the $^{13}CH_3$ relaxation data indicates that most of the methyl groups with decreased dynamics upon complex formation are those of Met and Leu residues[7]. Intermediate $^3J_{CC}$ couplings involving these methyl groups and very small $^1D_{CH}$ values confirm that all Met residues exhibit extensive dynamic averaging about χ_3. Similarly, four out of nine Leu residues show evidence for partial averaging around χ_2 (Fig. 4c,d).

How flexible are the CaM domains?

For apo CaM, NMR relaxation data provide strong evidence that the C-terminal domain exists in a dynamic equilibrium between its regular, closed apo state and an open conformation that is similar to that of the Ca^{2+}-ligated state[34]. The question then arises whether a similar situation exists in the N-terminal domain of Ca^{2+}–CaM, with the solution structure reported here representing the time-averaged structure between a dominant, open form and a small fraction of closed apo structure.

Table 1 Structural statistics and atomic r.m.s. differences[1]

Structural statistics		N-dom. (5–75)	C-dom. (82–146)
R.m.s. deviation[2,3] (Hz)			
Backbone (323 / 305)		1.70	1.42
NH	(66 / 65)	1.28	1.16
CαHα	(65 / 60)	2.09	1.62
C'Cα	(69 / 65)	1.55	1.21
NC'	(64 / 60)	1.56	1.53
C'Hα	(59 / 55)	1.29	1.50
Side chain			
CβHβ	(25 / 25)	2.83	2.44
CH$_3$	(13 / 10)	3.65	3.51
Deviations from idealized covalent geometry			
Bonds (Å)		0.0027	0.0024
Angles (°)		0.42	0.35
Impropers (°)		0.39	0.40
Energy (kcal mol^{-1})			
Dipolar		214	158
Dihedral		0.9	0.8
H-bond		0.8	0.7
Repel		50	43
ϕ / ψ in most favored region (%)[4]		93.3	96.6
Q_{free} (%)		18	20
Atomic r.m.s. differences (Å)[1]			
Backbone		0.28	0.26
All atoms		0.87	0.90

[1]Statistics are calculated and averaged over three simulated annealing structures, obtained from the three-stage protocol (see Methods) using three different starting structures. The precision of the atomic coordinates is defined as the average r.m.s. differences between the three final structures and their mean coordinates.
[2]From experimental dipolar coupling restraints. The r.m.s. difference between individual sets of experimental dipolar couplings and those predicted by refined structures (averaged over three final structures) by means of SVD fit. All couplings are normalized to $^1D_{NH}$.
[3]Values in parentheses correspond to the number of restraints for the N- and C-terminal domains.
[4]As evaluated with the program PROCHECK[50].

However, we do not believe transient closing of the Ca^{2+}-ligated domains to be the reason for the intermediate, 'almost open' conformation seen in the solution Ca^{2+}–CaM structure for three reasons. First, in contrast to apo CaM, there is no large scale conformational-exchange broadening in the N-terminal domain. Second, when optimizing a fit between the experimental dipolar couplings and an arbitrary linear combination of apo CaM and the X-ray structure of Ca^{2+}–CaM, the improvement in the correlation coefficient ($R_{SVD} = 0.95$) is lower than expected for such a dynamic equilibrium. Third, in this fit, the optimal ratio corresponds to 28% apo CaM and 72% Ca^{2+}–CaM. However, very strong interhelical NOE interactions in the apo state are observed involving the tips of the EF hand helices (for example, Leu 39-Cδ_2H$_3$ to Ala 15-CβH$_3$; Ala 15-CβH$_3$ to Val 35-Cγ_1H$_3$; and Val 35-Cγ_2H$_3$ to Phe 19-CδH)[13]. If this apo state were occupied 28% of the time in a dynamic equilibrium of the open and closed states, these interactions should yield substantial NOEs. However, even at the noise threshold, none of these interactions are observed (data not shown). Therefore, we conclude that the apo structure is not significantly occupied (<5%) under the solution conditions used in our experiments.

Large fluctuations in relative orientations can be detected by a separate fit of an alignment tensor for each well-defined, stable element of secondary structure[35]. However, when compar-

articles

Table 2 Interhelical angles in calmodulin[1,2]

	I–II	III–IV	V–VI	VII–VIII	PDB entry (ref.)
Ca^{2+}-ligated NMR	76 ± 2	78 ± 2	70 ± 2	78 ± 2	
Ca^{2+}-free NMR	50 ± 2	48 ± 2	38 ± 2	53 ± 2	1F70, 1F71 (25)
Paramecium	91	96	75	89	1EXR (17)
Human	92	93	75	85	1CLL (24)
RLC C-domain			70	73	1WDC (30)
ELC C-domain			66	87	1WDC (30)
CaM–smMLCK	91	98	81	82	1 CDL (10)
CaM–CaMKII	89	87	83	94	1 CDM (11)

[1]The interhelical angles are calculated using the algorithm of Kuboniwa *et al.*[13]
[2]Structures were determined by X-ray crystallography unless indicated otherwise.

ing the relative magnitude of the alignment tensor for each of the four helices, very similar values are obtained with relative differences not much larger than when comparing the fit of dipolar couplings in a given helix with different Ca^{2+}–CaM crystal structures. Calculations indicate that for harmonic oscillation of an α-helix across an arc, a significant effect on its alignment tensor is expected when the oscillation amplitude exceeds ±25°. The various dipolar couplings then scale by factors that depend on the angle between the dipolar interaction vector and the pivot axis, intrinsically containing information about the direction and magnitude of the motion. The calculations also show that such effects become essentially undetectable below an amplitude of ±20°, thereby putting an approximate upper limit on the magnitude of such oscillations in CaM.

As judged by the substantial differences between the solution and the crystal structures of free Ca^{2+}–CaM or its complexes with target peptides, substantial flexibility remains in the Ca^{2+}-saturated state. The anisotropy of the B-factors of the 1 Å crystal structure also point at a scissor-type motion within each EF hand but does not provide a handle on the magnitude of such oscillations in solution. Considering that the dipolar couplings reflect the time-averaged orientation, the difference in structure between the solution and crystalline states indicates that this amplitude can be rather large.

Concluding remarks

The utility of dipolar couplings to identify the effect of crystal packing on structure has been demonstrated for several multidomain proteins, including maltose binding protein and T4 lysozyme[28,36]. However, the conformations of domains themselves are usually assumed to be so rigid that they are not significantly affected by crystal packing or the conditions used for crystallizing the protein. Ca^{2+}–CaM is clearly an exception to this rule. Not only is the relative orientation of the N- and C-terminal domains nearly random in solution, the interhelical angles in the N-terminal domain also differ by as much as 25° from what is seen in the crystalline state. Clearly, not only do the hydrophobic clefts, which are lined with flexible Met residues, provide a pliable interaction surface, the relative helix orientations are also easily changed in order to optimize target binding.

Analysis of $^3J_{CC}$ and $^3J_{CN}$ couplings in Ca^{2+}–CaM shows that a single χ$_1$ rotamer is predominately (>75%) occupied for the majority of residues; from this group, all but three Glu residues adopt the same χ$_1$ as found in the 1 Å crystal structure. In contrast, high flexibility and little correlation to the X-ray data are

observed for the Met χ$_3$ rotameric states. Leu and Ile χ$_2$ angles are largely intermediate in this respect. Clearly, the high degree of Met flexibility combined with the pliability of the relative helix angles are the primary reasons for the ability of calmodulin to bind to such a wide range of target shapes[37].

From a methodological perspective, we argue that the difference between the solution and crystal structures of the N-terminal domain can be characterized accurately only by dipolar couplings. Analysis shows moving from 1EXR to the refined structure results in <0.5 Å as the largest change in any NOE distance (using a 4 Å cutoff). Thus, accurately defining the interhelix orientation from NOE distances alone without going through exceptional care in quantitating these distances is impossible. Clearly, the dipolar coupling approach is uniquely suited to evaluate relatively subtle structural changes, which may have profound implications on understanding molecular recognition. Because analysis of dipolar and J coupling data is a linear task, which does not require identification of interaction partners in contrast to NOE analysis, it is a very fast process that is easily automated. The main time required for such a study is, therefore, the measurement of the couplings themselves (~3 d each for the backbone couplings in isotropic and liquid crystalline samples, and a total of 2 d for the side chain-related couplings). This suggests that the dipolar coupling approach used in this study will be valuable in applications to structural genomics, particularly when low resolution homology models are available.

Methods

NMR measurement. Uniformly ^{15}N- and ^{13}C-labeled recombinant *Xenopus* calmodulin (CaM) was overexpressed in *Escherichia coli* (strain AR58) and purified to homogeneity as described[8]. A total of three NMR samples was used for the present study, each prepared in 250 µl of 95% (v/v) H$_2$O / 5% D$_2$O, pH 7.0, using 280 µl Shigemi microcells. The isotropic sample contains 1 mM CaM, 16 mM CaCl$_2$ and 100 mM KCl. The aligned sample used for structure determination contains 15 mg ml^{-1} of the filamentous phage Pf1 (Asla Labs, *http://130.237.129.141//asla/asla-phage.htm*), 1 mM CaM, 16 mM CaCl$_2$ and 10 mM KCl. A second aligned sample was also made, containing 18 mg ml^{-1} Pf1, 0.5 mM CaM, 6 mM CaCl$_2$ and 100 mM KCl. All NMR experiments were conducted on Bruker spectrometers at 32 °C. At 10 mM KCl, the amide chemical shifts of CaM in Pf1 liquid crystal are virtually identical to that of the isotropic sample, indicating that perturbation of the protein by the alignment medium is minimal, as expected on the basis of repelling interactions between negatively charged Pf1 and negative Ca^{2+}–CaM.

Five types of backbone dipolar couplings were measured: $^1D_{NH}$, $^1D_{C\alpha H\alpha}$, $^1D_{C'C\alpha}$, $^1D_{C'N}$ and $^1D_{C'H\alpha}$. The ^1H-^{15}N couplings were measured at 600 MHz (^1H frequency) using three-dimensional (3D) HNCO[38], recorded with 50 ms of ^1H-coupled mixed-CT ^{15}N evolution. Both $^1H\alpha$-$^{13}C\alpha$ and $^1H\beta$-$^{13}C\beta$ couplings were simultaneously obtained at 600 MHz by quantitative J correlation extracted from the CBCA(CO)NH experiment[39]. The $^{13}C'$-$^{13}C\alpha$ couplings were conveniently obtained at 500 MHz from the standard 3D HNCO recorded with 120 ms of $^{13}C\alpha$-coupled $^{13}C'$ evolution and using a cryoprobe to enhance sensitivity and accuracy of the $^1D_{C'C\alpha}$ measurement. The small one-bond $^{13}C'$-^{15}N couplings were measured at 750 MHz using the 3D TROSY-HNCO in a quantitative-J manner[40]. Finally, the two-bond $^{13}C'$-$^1H\alpha$ couplings were obtained at 500 MHz using a HNCOCA type of pulse scheme[35]. Couplings were extracted from addition and subtraction of the in-phase and antiphase $^{13}C'$-$^1H\alpha$ spectra. On the basis of the length of the time domain data and the signal-to-noise[41] ratio, the accuracy of the measured dipolar couplings is estimated at ±0.2 Hz ($^1D_{NH}$), ±0.1 Hz ($^1D_{C'C\alpha}$) and ±0.25 Hz ($^1D_{C'H\alpha}$). For those couplings derived from quantitative J experiments, the estimated errors are ±2.4 Hz ($^1D_{C\alpha H\alpha}$), ±1.6 Hz ($^1D_{C\beta H\beta}$), and ±0.2 Hz ($^1D_{NC'}$). Measurement of $^1D_{CH_3}$ couplings in CaM has been reported[42].

articles

$^3J_{CC}$ and $^3J_{CN}$ coupling measurements for determination of side chain couplings were carried out at 600 MHz for couplings involving $^{13}C'$ and at 800 MHz for all other couplings, using standard two-dimensional methods[43].

To search for apo-specific NOESY crosspeaks, the ^{13}C-separated 3D NOESY spectrum of the isotropic sample was recorded with 100 ms NOE mixing at 750 MHz. All NMR spectra were processed and analyzed using NMRPipe[44] and NMRDraw[44].

Fitting of dipolar couplings. Fits of the dipolar couplings to structures were done by singular value decomposition using SSIA[29]. The SVD routine was also modified in order to fit a linear combination of two structures. Proton coordinates were added to the X-ray structures by X-PLOR[45], enforcing the common NMR topology. The internuclear distances were assumed fixed at 1.041 Å (N-H), 1.329 Å (N-C'), 1.526 Å (Cα-C') and 1.117 Å (Cα-Hα)[46]. For the C'-Hα interaction, a distance of 2.144 Å was used.

The alignment tensor magnitude and orientation at 100 mM KCl, 18 mg ml^{-1} Pf1 differs significantly from values at 10 mM KCl, 15 mg ml^{-1} Pf1. For the C-terminal domain, D_a changes from +10.1 Hz at 10 mM KCl to –11.6 Hz at 100 mM KCl, whereas the rhombicity, R, decreases from 0.66 to 0.49. For the N-terminal domain, D_a decreases from +11.0 to +10.2 Hz and R increases from 0.38 to 0.47.

Structure calculation protocol. The three-stage structure calculation protocol is based on simulated annealing at very low temperature using X-PLOR[45]. In stage one, ϕ and ψ backbone torsion angle restraints extracted from the starting model are enforced by strong harmonic quadratic potentials with a force constant fixed at 300 kcal mol^{-1} rad^{-2}. For side chains that are 'locked' into nearly ideal χ$_1$ staggered rotamers on the basis of $^3J_{C'Cγ}$ and $^3J_{NCγ}$ couplings, as well as comparing $^1Hβ$-$^{13}Cβ$, $^1Hα$-$^{13}Cα$ and $^{13}C'$-$^{13}Cα$ dipolar couplings[25], flat-well (±30°) harmonic χ$_1$ and χ$_2$ angle potentials (50 kcal mol^{-1} rad^{-2}) are used. Additionally, a weak database-derived 'Rama' potential function[47] in X-PLOR is ramped from 0.02 to 0.2 (dimensionless force constant) for the general treatment of side chain rotamers. O-HN and O-N hydrogen bond distance restraints of 1.9 and 2.9 Å, respectively, in well-defined secondary structure elements are enforced with flat-well (±0.2 Å) harmonic potentials, with the force constant ramped exponentially from 25 to 50 kcal mol^{-1} Å^{-2}. For the N-terminal domain, the hydrogen bond restraints are applied for α-helical residues 6–18, 29–38, 45–54 and 65–74, and a pair of H-bonds between Ile 27 and Ile 63 forming the short antiparallel β-sheet. Likewise in the C-terminal domain, helical restraints are included for 83–91, 102–111, 118–127 and 139–145, and the mini-β-sheet H-bonds between Ile 100 and Val 136. Removal of all hydrogen bond restraints does not alter the structure significantly but results in slightly extended helices, presumably as a result of the strictly enforced covalent bond angles that differ slightly from those seen in α-helices. The positions of Ca^{2+} ions are defined by restraining their distance to 2.4 ± 0.1 Å from the known ligating oxygens. Removal of these restraints has no effect on the backbone but alters the χ$_1$ of several otherwise unrestrained Asp side chains.

Dipolar couplings do not provide translational information, and a pseudo potential for the radius of gyration (RG)[48] is applied with a fixed force constant of 50 kcal mol^{-1} Å^{-2} to counteract the natural tendency of proteins to expand during simulated annealing runs owing to the repulsive van der Waals term. Turning off this term had no noticeable effect (<2°) on the interhelical angles but yields slightly expanded structures (backbone r.m.s. deviation 0.6 Å relative to structures with RG). A detailed description of the refinement protocol is presented elsewhere[25]. Final structures are calculated using all five sets of backbone dipolar couplings and side chain dipolar couplings for sites where the absence of rotamer averaging is indicated by $^3J_{CC}$ and $^3J_{CN}$.

Coordinates. Atomic coordinates have been deposited in the Protein Data Bank (accession codes 1J7O and 1J7P correspond to the structures of the N- and C-terminal domains, respectively, of CaM).

articles

1. Cohen, P. & Klee, C.B. *Calmodulin* (Elsevier, New York; 1988).
2. Crivici, A. & Ikura, M. Molecular and structural basis of target recognition by calmodulin. *Annu. Rev. Biophys. Biomolec. Struct.* **24**, 85–116 (1995).
3. Chin, D. & Means, A.R. Calmodulin: a prototypical calcium sensor. *Trends Cell Biol.* **10**, 322–328 (2000).
4. Babu, Y.S., Bugg, C.E. & Cook, W.J. Structure of calmodulin refined at 2.2 Å resolution. *J. Mol. Biol.* **204**, 191–204 (1988).
5. Kretsinger, R.H. & Nockolds, C.E. Carp muscle calcium-binding protein. II. Structure determination and general description. *J. Biol. Chem.* **248**, 3313–3326 (1973).
6. Osawa, M. *et al.* Solution structure of calmodulin-W-7 complex: the basis of diversity in molecular recognition. *J. Mol. Biol.* **276**, 165–176 (1998).
7. Lee, A.L., Kinnear, S.A. & Wand, A.J. Redistribution and loss of side chain entropy upon formation of a calmodulin-peptide complex. *Nature Struct. Biol.* **7**, 72–77 (2000).
8. Barbato, G., Ikura, M., Kay, L.E., Pastor, R.W. & Bax, A. Backbone dynamics of calmodulin studied by ^{15}N relaxation using inverse detected two-dimensional NMR spectroscopy: the central helix is flexible. *Biochemistry* **31**, 5269–5278 (1992).
9. Ikura, M. *et al.* Solution structure of a calmodulin-target peptide complex by multidimensional NMR. *Science* **256**, 632–638 (1992).
10. Meador, W.E., Means, A.R. & Quiocho, F.A. Target enzyme recognition by calmodulin: 2.4 Å structure of a calmodulin-peptide complex. *Science* **257**, 1251–1254 (1992).
11. Meador, W.E., Means, A.R. & Quiocho, F.A. Modulation of calmodulin plasticity in molecular recognition on the basis of X-ray structures. *Science* **262**, 1718–1721 (1993).
12. Tjandra, N., Kuboniwa, H., Ren, H. & Bax, A. Rotational dynamics of calcium-free calmodulin studied by ^{15}N-NMR relaxation measurements. *Eur. J. Biochem.* **230**, 1014–1024 (1995).
13. Kuboniwa, H. *et al.* Solution structure of calcium-free calmodulin. *Nature Struct. Biol.* **2**, 768–776 (1995).
14. Zhang, M., Tanaka, T. & Ikura, M. Calcium-induced conformational transition revealed by the solution structure of apo calmodulin. *Nature Struct. Biol.* **2**, 758–767 (1995).
15. Finn, B.E. *et al.* Calcium-induced structural-changes and domain autonomy in calmodulin. *Nature Struct. Biol.* **2**, 777–783 (1995).
16. Herzberg, O. & James, M.N.G. Structure of the calcium regulatory muscle protein troponin-C at 2.8-Å resolution. *Nature* **313**, 653–659 (1985).
17. Wilson, M.A. & Brünger, A.T. The 1.0 Å crystal structure of Ca²⁺-bound calmodulin: an analysis of disorder and implications for functionally relevant plasticity. *J. Mol. Biol.* **301**, 1237–1256 (2000).
18. Ikura, M. *et al.* Secondary structure and side-chain ^{1}H and ^{13}C resonance assignments of calmodulin in solution by heteronuclear multidimensional NMR-spectroscopy. *Biochemistry* **30**, 9216–9228 (1991).
19. Tjandra, N., Garrett, D.S., Gronenborn, A.M., Bax, A. & Clore, G.M. Defining long range order in NMR structure determination from the dependence of heteronuclear relaxation times on rotational diffusion anisotropy. *Nature Struct. Biol.* **4**, 443–449 (1997).
20. Cornilescu, G., Marquardt, J.L., Ottiger, M. & Bax, A. Validation of protein structure from anisotropic carbonyl chemical shifts in a dilute liquid crystalline phase. *J. Am. Chem. Soc.* **120**, 6836–6837 (1998).
21. Clore, G.M. & Garrett, D.S. R-factor, free R, and complete cross-validation for dipolar coupling refinement of NMR structures. *J. Am. Chem. Soc.* **121**, 9008–9012 (1999).
22. Ottiger, M. & Bax, A. Bicelle-based liquid crystals for NMR-measurement of dipolar couplings at acidic and basic pH values. *J. Biomol. NMR* **13**, 187–191 (1999).
23. Hansen, M.R., Mueller, L. & Pardi, A. Tunable alignment of macromolecules by filamentous phage yields dipolar coupling interactions. *Nature Struct. Biol.* **5**, 1065–1074 (1998).
24. Chattopadhyaya, R., Meador, W.E., Means, A.R. & Quiocho, F.A. Calmodulin structure refined at 1.7 Å resolution. *J. Mol. Biol.* **228**, 1177–1192 (1992).
25. Chou, J.J., Li, S. & Bax, A. Study of conformational rearrangement and refinement of structural homology models by the use of dipolar couplings. *J. Biomol. NMR* **18**, 217–227 (2000).
26. Levitt, M. Accurate modeling of protein conformation by automatic segment matching. *J. Mol. Biol.* **226**, 507–533 (1992).
27. Tjandra, N., Tate, S., Ono, A., Kainosho, M. & Bax, A. The NMR structure of a DNA dodecamer in an aqueous dilute liquid crystalline phase. *J. Am. Chem. Soc.* **122**, 6190–6200 (2000).
28. Goto, N.K., Skrynnikov, N.R., Dahlquist, F.W. & Kay, L.E. What is the average conformation of T4 lysozyme in solution? A domain orientation study using dipolar couplings measured by solution NMR. *J. Mol. Biol.* **308**, 745–764 (2001).
29. Zweckstetter, M. & Bax, A. Prediction of sterically induced alignment in a dilute liquid crystalline phase: aid to protein structure determination by NMR. *J. Am. Chem. Soc.* **122**, 3791–3792 (2000).
30. Houdusse, A. & Cohen, C. Structure of the regulatory domain of scallop myosin at 2 Å resolution: implications for regulation. *Structure* **4**, 21–32 (1996).
31. Tabernero, L. *et al.* The structure of a calmodulin mutant with a deletion in the central helix: implications for molecular recognition and protein binding. *Structure* **5**, 613–622 (1997).
32. Yuan, T. & Vogel, H.J. Substitution of the methionine residues of calmodulin with the unnatural amino acid analogs ethionine and norleucine: biochemical and spectroscopic studies. *Protein Sci.* **8**, 113–121 (1999).
33. Hu, J.S., Grzesiek, S. & Bax, A. Two-dimensional NMR methods for determining (χ_1) angles of aromatic residues in proteins from three-bond $J_{C'C\gamma}$ and $J_{NC\gamma}$ couplings. *J. Am. Chem. Soc.* **119**, 1803–1804 (1997).
34. Malmendal, A., Evenas, J., Forsen, S. & Akke, M. Structural dynamics in the C-terminal domain of calmodulin at low calcium levels. *J. Mol. Biol.* **293**, 883–899 (1999).
35. Tolman, J.R., Al-Hashimi, H.M., Kay, L.E. & Prestegard, J.H. Structural and dynamic analysis of residual dipolar coupling data for proteins. *J. Am. Chem. Soc.* **123**, 1416–1424 (2001).
36. Skrynnikov, N.R. *et al.* Orienting domains in proteins using dipolar couplings measured by liquid-state NMR: differences in solution and crystal forms of maltodextrin binding protein loaded with β-cyclodextrin. *J. Mol. Biol.* **295**, 1265–1273 (2000).
37. Yap, K.L., Ames, J.B., Swindells, M.B. & Ikura, M. Diversity of conformational states and changes within the EF-hand protein superfamily. *Prot. Struct. Funct. Genet.* **37**, 499–507 (1999).
38. Ikura, M., Kay, L.E. & Bax, A. A novel approach for sequential assignment of ^{1}H, ^{13}C, and ^{15}N spectra of larger proteins: heteronuclear triple-resonance three-dimensional NMR spectroscopy. Application to calmodulin. *Biochemistry* **29**, 4659–4667 (1990).
39. Chou, J.J. & Bax, A. Protein side chain rotamers from dipolar couplings in a liquid crystalline phase. *J. Am. Chem. Soc.* **123**, 3844–3845 (2001).
40. Chou, J.J., Delaglio, F. & Bax, A. Measurement of one-bond ^{15}N-^{13}C′ dipolar couplings in medium sized proteins. *J. Biomol. NMR* **18**, 101–105 (2000).
41. Kontaxis, G., Clore, G.M. & Bax, A. Evaluation of cross-correlation effects and measurement of one-bond couplings in proteins with short transverse relaxation times. *J. Magn. Reson.* **143**, 184–196 (2000).
42. Kontaxis, G. & Bax, A. Multiplet component separation for measurement of methyl ^{13}C- ^{1}H dipolar couplings in weakly aligned proteins. *J. Biomol. NMR* **20**, 77–82 (2001).
43. Bax, A. *et al.* Measurement of homonuclear and hteronuclear J-couplings from quantitative J-correlation. *Methods Enzymol.* **239**, 79–105 (1994).
44. Delaglio, F. *et al.* NMRPipe - a multidimensional spectral processing system based on Unix pipes. *J. Biomol. NMR* **6**, 277–293 (1995).
45. Brunger, A.T. *X-PLOR: A system for X-ray crystallography and NMR* (Yale University Press, New Haven; 1993).
46. Ottiger, M. & Bax, A. Determination of relative N-H-N N-C′, Cα-C′, and Cα-Hα effective bond lengths in a protein by NMR in a dilute liquid crystalline phase. *J. Am. Chem. Soc.* **120**, 12334–12341 (1998).
47. Kuszewski, J., Gronenborn, A.M. & Clore, G.M. Improvements and extensions in the conformational database potential for the refinement of NMR and X-ray structures of proteins and nucleic acids. *J. Magn. Reson.* **125**, 171–177 (1997).
48. Kuszewski, J., Gronenborn, A.M. & Clore, G.M. Improving the packing and accuracy of NMR structures with a pseudopotential for the radius of gyration. *J. Am. Chem. Soc.* **121**, 2337–2338 (1999).
49. Koradi, R., Billeter, M. & Wuthrich, K. MOLMOL: a program for display and analysis of macromolecular structures. *J. Mol. Graph.* **14**, 51–55 (1996).
50. Laskowski, R.A., MacArthur, M.W., Moss, D.S. & Thornton, J.W. PROCHECK: a program to check the stereochemical quality of protein structures. *J. Appl. Crystallogr.* **26**, 283–291 (1993).